Microscopic analysis of ^{10,11}Be elastic scattering on protons and nuclei, and breakup processes of ^{11}Be within the ^{10}Be + n cluster model

V. K. Lukyanov,[1] D. N. Kadrev,[2] E. V. Zemlyanaya,[1] K. Spasova,[2,3] K. V. Lukyanov,[1] A. N. Antonov,[2] and M. K. Gaidarov[2]
[1]*Joint Institute for Nuclear Research, Dubna 141980, Russia*
[2]*Institute for Nuclear Research and Nuclear Energy, Bulgarian Academy of Sciences, Sofia 1784, Bulgaria*
[3]*"Bishop K. Preslavski" University, Shumen 9712, Bulgaria*
(Received 19 January 2015; published 9 March 2015)

The density distributions of ^{10}Be and ^{11}Be nuclei obtained within the quantum Monte Carlo model and the generator coordinate method are used to calculate the microscopic optical potentials (OPs) and cross sections of elastic scattering of these nuclei on protons and ^{12}C at energies $E < 100$ MeV/nucleon. The real part of the OP is calculated using the folding model with the exchange terms included, while the imaginary part of the OP that reproduces the phase of scattering is obtained in the high-energy approximation. In this hybrid model of OP the free parameters are the depths of the real and imaginary parts obtained by fitting the experimental data. The well-known energy dependence of the volume integrals is used as a physical constraint to resolve the ambiguities of the parameter values. The role of the spin-orbit potential and the surface contribution to the OP is studied for an adequate description of available experimental elastic scattering cross-section data. Also, the cluster model, in which ^{11}Be consists of a n-halo and the ^{10}Be core, is adopted. Within the latter, the breakup cross sections of ^{11}Be nucleus on ^{9}Be, ^{93}Nb, ^{181}Ta, and ^{238}U targets and momentum distributions of ^{10}Be fragments are calculated and compared with the existing experimental data.

DOI: 10.1103/PhysRevC.91.034606 PACS number(s): 25.40.Cm, 24.10.Ht, 25.60.Gc, 21.10.Gv

I. INTRODUCTION

The discovery of halo nuclei [1] has been related to the measured interaction cross sections of nuclei like ^{6,8}He, ^{11}Li, and Be isotopes with various target nuclei [2–6]. The evidence of the existence of an extended halo in neutron-rich nuclei is based on the observed unusually narrow momentum distribution of a core fragment and enhanced reaction cross section. The first example was the breakup of ^{11}Li at high energies [7–10] by observing the large interaction reaction cross section [2] and the narrow momentum distribution of ^{9}Li in the breakup of ^{11}Li, e.g., in the reaction $^{11}\text{Li} + {}^{12}\text{C}$ at $E = 800$ MeV/nucleon [7]. Here we should mention also the results of the experiments at lower energies ($E = 60$ MeV/nucleon) of scattering of ^{11}Li on ^{9}Be, ^{93}Nb, and ^{181}Ta [11] and of ^{11}Li on a wide range of nuclei from ^{9}Be to ^{238}U [12]. As shown in Ref. [13], not only scattering but also the breakup of ^{11}Be in the collisions with the target nuclei ^{93}Nb, ^{181}Ta, and ^{238}U play decisive roles when studying the internal cluster structure of ^{11}Be. Indeed, the narrow peak of the momentum distributions of the breakup fragments of such a neutron-rich nucleus reflects the very large extension of its wave function, compared to that of the core nucleus ^{10}Be, and thus evidences the existence of the nuclear halo [14–20]. As was concluded in Ref. [18], namely the longitudinal component of the momentum (taken along the beam or the z direction) provides the most accurate information on the intrinsic properties of the halo, being insensitive to details of the collision and the size of the target. In addition, recent measurements of the charge radii of ^{7,9,10,11}Be pointed out that the average distance between the halo neutrons and the ^{10}Be dense core of the ^{11}Be nucleus is around 7 fm [21]. Thus, the halo neutron is about three times as far from the dense core as is the outermost proton because the core itself has a radius of only 2.5 fm.

An important finding when investigating reactions with ^{10}Be and ^{11}Be nuclei, in particular the $^{10}\text{Be} + n$ breakup of ^{11}Be, is the effect of the deformed ^{10}Be core on the two-body cluster structure of ^{11}Be. In fact, in the ^{11}Be nucleus the inversion of the $p_{1/2}$ and $s_{1/2}$ orbitals predicted by Talmi and Unna [22] and confirmed by Alburger *et al.* [23] leads to a $1/2^+$ ground state. Also, the probability of the $E1$ transition from this ground state to the $1/2^-$ first excited state of ^{11}Be located at 320 keV excitation energy is the largest ever measured in light nuclei [24,25]. The effects of the core deformation on the breakup of ^{11}Be on protons have been studied in several works. For example, in addition to a two-body cluster structure with an inert $^{10}\text{Be}e(0^+)$ core and a valence neutron used in Ref. [26] in the continuum discretized coupled-channels (CDCC) calculations of elastic and inelastic proton scattering on ^{11}Be, the authors have also discussed the necessity to account for contributions from configurations involving excited states of the ^{10}Be core to the $^{10}\text{Be} + n$ continuum of ^{11}Be. Crespo *et al.* [27] have found that the core excitation $p + {}^{10}\text{Be}(0_1^+) \rightarrow p + {}^{10}\text{Be}(2_1^+)$ provides a significant contribution to the breakup cross section of ^{11}Be on the proton target at 63.7 MeV/nucleon incident energy.

In the earlier works (e.g., Ref. [28]) the elastic scattering cross sections of ^{10,11}Be on protons have been calculated using phenomenological OPs of given forms with numerous fitting parameters of their real (ReOP) and imaginary (ImOP) parts. However, in the further calculations the more physically motivated microscopic folding models were applied (see, e.g., Refs. [29–32]). In many works [30–32] the folding procedure was explored for the real part of the OP. Within the latter procedure the direct and exchange parts of the ReOP with effective nucleon-nucleon forces are calculated. At the same time the OP is usually taken in a phenomenological form. Many successful applications of this model have been made

for the proton- and nucleus-nucleus collisions (see, e.g., cycles of works [31,33,34]). This model was also explored in Refs. [35,36] for the scattering of ^{10,11}Be + p, where the exchange part of the folded ReOP is taken in the form of the zero-range prescription and the density distribution of ^{11}Be has the Gaussian-oscillator form. In the recent work [37] the authors account for the full exchange part of the ReOP, while the ImOP was calculated using the folding high-energy approximation (HEA) formula from Refs. [38,39]. In Refs. [37,40] a surface term to the ImOP was added to improve the agreement with the data at lower energies.

In our present work, as well as in our previous works considering processes with exotic He and Li isotopes [41–44], we use microscopically calculated OPs within the hybrid model [38]. In the latter the ReOP is calculated by a folding of a nuclear density and the effective NN potentials [32] (see also Ref. [45]) and includes both direct and exchange parts. The ImOP is obtained within the HEA model [46,47]. There are only two or three fitting parameters in the hybrid model that are related to the depths of the ReOP, ImOP, and the spin-orbit part of the OP. Along with some phenomenological density distributions for He and Li isotopes, we have used in our works realistic microscopic density obtained within the large-scale shell model (LSSM) [48,49]. In the present work, devoted to processes with ^{10,11}Be nuclei, we use the density distribution for ^{10}Be obtained within the quantum Monte Carlo (QMC) model [50,51] and also the densities of ^{10}Be and ^{11}Be obtained within the generator coordinate method (GCM) [52].

The main aim of our work is twofold. First, we study the elastic scattering of the neutron-rich exotic ^{10}Be and ^{11}Be nuclei on protons and nuclei at energies $E < 100$ MeV/nucleon using real and imaginary parts of the optical potentials microscopically calculated in our work. Second, we estimate important characteristics of the reactions with ^{11}Be, such as the breakup cross sections and momentum distributions of fragments in breakup processes. To this end we use the model in which ^{11}Be consists of a core of ^{10}Be and a halo formed by a motion of a neutron in its periphery (e.g., Refs. [53–55]). The latter model is justified by the small separation energy $S_n = 504 \pm 6$ KeV of a neutron from the ground $s_{1/2}$ state of ^{11}Be [56] and on the observed quite-large total interaction cross sections of ^{11}Be with target nuclei caused by the main contribution from the breakup of ^{11}Be on ^{10}Be and a neutron. The important role of the periphery is confirmed also by the experiments on scattering of ^{11}Be on the heavy nucleus of ^{208}Pb [57], where the prevailing mechanism is the direct breakup owing to the long-range Coulomb force of the nucleus. Also we should mention the important observation of the narrow peak in the momentum distribution of the ^{10}Be fragments at the breakup of ^{11}Be scattering on the ^{12}C nucleus [13], that is, as mentioned above, a consequence of the large extension of the wave function of the relative motion in the ^{10}Be + n system related to the small neutron separation energy. By means of such a cluster model of ^{11}Be one can calculate the OPs for scattering of ^{11}Be on protons or nuclear targets. To this end one should use the known $n + p$ potential and calculate using the microscopic model the optical potentials of ^{10}Be + p (or ^{10}Be + A and the $n + A$ potentials). Then the sum of these potentials is folded with a density probability of the relative motion of the core ^{10}Be and the neutron. Also, in the framework of this cluster model one can calculate the momentum distribution of ^{10}Be fragments from the breakup reactions ^{11}Be + ^{9}Be, ^{11}Be + ^{93}Nb, ^{11}Be + ^{181}Ta, and ^{11}Be + ^{238}U, for which experimental data are available.

The structure of the paper is as follows. The theoretical scheme to calculate microscopically within the hybrid model the ReOP, the ImOP, the spin-orbit part of the OP, and the surface component of OP, as well as the results of the calculations of the elastic scattering cross sections of ^{10,11}Be + p and ^{10,11}Be + ^{12}C, are presented in Sec. II. The basic expressions to estimate the breakup of ^{11}Be and to calculate the cross sections and the fragment momentum distributions of ^{10}Be in the diffraction and stripping processes of ^{11}Be on ^{9}Be, ^{93}Nb, ^{181}Ta, and ^{238}U are given in Sec. III. The summary and conclusions of the work are included in Sec. IV.

II. ELASTIC SCATTERING OF ^{10,11}Be ON PROTONS AND ^{12}C AT $E < 100$ MeV/NUCLEON

A. Hybrid model of the microscopic optical potential

In the present work we calculate the microscopic OP that contains the volume real ($V^{\rm F}$) and imaginary parts (W) and the spin-orbit interaction (V^{ls}). This OP is used for calculations of elastic scattering differential cross sections. We introduce a set of weighting coefficients $N_{\rm R}$, $N_{\rm I}$, $N_{\rm R}^{ls}$, and $N_{\rm I}^{ls}$ that are related to the depths of the corresponding parts of the OP and are obtained by a fitting procedure to the available experimental data. Details of the constructing of the OP are given in Refs. [30–32,45]. The OP has the form

$$U(r) = N_{\rm R} V^{\rm F}(r) + i N_{\rm I} W(r) - 2\lambda_\pi^2 \left[N_{\rm R}^{ls} V_{\rm R}^{ls} \frac{1}{r}\frac{df_{\rm R}(r)}{dr} + i N_{\rm I}^{ls} W_{\rm I}^{ls} \frac{1}{r}\frac{df_{\rm I}(r)}{dr} \right] (\vec{l}\cdot\vec{s}), \quad (1)$$

where $2\lambda_\pi^2 = 4$ fm^2 with the squared pion Compton wavelength $\lambda_\pi^2 = 2$ fm^2. Let us denote the values of the ReOP and ImOP at $r = 0$ by $V_{\rm R}[\equiv V^{\rm F}(r=0)]$ and $W_{\rm I}[\equiv W(r=0)]$. We note that the spin-orbit part of the OP contains real and imaginary terms with the parameters $V_{\rm R}^{ls}$ and $W_{\rm I}^{ls}$ related to $V_{\rm R}$ and $W_{\rm I}$ by $V_{\rm R}^{ls} = V_{\rm R}/4$ and $W_{\rm I}^{ls} = W_{\rm I}/4$, correspondingly. Here $V_{\rm R}$ and $W_{\rm I}$ (and $V_{\rm R}^{ls}$ and $W_{\rm I}^{ls}$) have to be negative. The ReOP $V^{\rm F}(r)$ is a sum of isoscalar ($V_{\rm IS}^{\rm F}$) and isovector ($V_{\rm IV}^{\rm F}$) components and each of them has its direct ($V_{\rm IS}^{\rm D}$ and $V_{\rm IV}^{\rm D}$) and exchanged ($V_{\rm IS}^{\rm EX}$ and $V_{\rm IV}^{\rm EX}$) parts.

The isoscalar component has the form

$$V_{\rm IS}^{\rm F}(r) = V_{\rm IS}^{\rm D}(r) + V_{\rm IS}^{\rm EX}(r) = \int d^3\mathbf{r}_p d^3\mathbf{r}_t \{\rho_p(\mathbf{r}_p)\rho_t(\mathbf{r}_t) v_{NN}^{D}(\mathbf{s}) + \rho_p(\mathbf{r}_p, \mathbf{r}_p+\mathbf{s})\rho_t(\mathbf{r}_t, \mathbf{r}_t-\mathbf{s}) v_{NN}^{\rm EX}(\mathbf{s}) \exp[\imath \mathbf{K}(r)\mathbf{s}/M]\}, \quad (2)$$

where $\mathbf{s} = \mathbf{r} + \mathbf{r}_t - \mathbf{r}_p$ is the vector between two nucleons, one of which belongs to the projectile and another one to the target nucleus.

In the first term of the right-hand side of Eq. (2) the densities of the incident particle ρ_p and the target nucleus ρ_t are sums of the proton and neutron densities. In the second term ρ_p and

ρ_t are the corresponding one-body density matrices. In our work we use for them the approximations for the knock-on exchange term of the folded potential from Refs. [58,59] (see also Refs. [41,43]). In Eq. (2) $\mathbf{K}(r)$ is the local momentum of the nucleus-nucleus relative motion and v_{NN}^{D} and v_{NN}^{EX} are the direct and exchange effective NN potentials. They contain an energy dependence usually taken in the form $g(E) = 1 - 0.003E$ and a density dependence with the form for the CDM3Y6 effective Paris potential [32],

$$F(\rho) = C[1 + \alpha e^{-\beta\rho(\mathbf{r})} - \gamma\rho(\mathbf{r})], \tag{3}$$

with $C = 0.2658$, $\alpha = 3.8033$, $\beta = 1.4099$ fm^3, and $\gamma = 4.0$ fm^3. The effective NN interactions v_{NN}^{D} and v_{NN}^{EX} have their isoscalar and isovector components in the form of M3Y interaction obtained within g-matrix calculations using the Paris NN potential [31,32]. The isovector components $V_{\mathrm{IV}}^{\mathrm{F}}$ of the ReOP can be obtained by exchanging in Eq. (2) the sum of the proton and neutron densities in $\rho_{p(t)}$ with their difference and using the isovector parts of the effective NN interaction. In the case of the proton scattering on nuclei, Eq. (2) contains only the density of the target nucleus.

The ImOP can be chosen either to be in the form of the microscopically calculated V^{F} ($W = V^{\mathrm{F}}$) or in the form W^{H} obtained in Ref. [38,39] within the HEA of the scattering theory [46,47]:

$$W^{\mathrm{H}}(r) = -\frac{\bar{\sigma}_N}{2\pi^2}\frac{E}{k}\int_0^\infty j_0(kr)\rho_p(q)\rho_t(q)f_N(q)q^2dq. \tag{4}$$

In Eq. (4) $\rho(q)$ are the corresponding form factors of the nuclear densities, $f_N(q)$ is the amplitude of the NN scattering and $\bar{\sigma}_N$ is the averaged over the isospin of the nucleus total NN scattering cross section that depends on the energy. The parametrization of the latter dependence can be seen, e.g., in Refs. [41,60]. We note that to obtain the HEA OP [with its imaginary part W^{H} in Eq. (4)] one can use the definition of the eikonal phase as an integral of the nucleon-nucleus potential over the trajectory of the straight-line propagation and has to compare it with the corresponding Glauber expression for the phase in the optical limit approximation. In the suggested scheme we use the nuclear densities and NN cross sections known from other sources and also the already-used NN potentials and amplitudes. In this way, the only free parameters in our approach are the parameters N that renormalize the depths of the OPs components. In the spin-orbit parts of the OP the functions $f_{\mathrm{I}}(r)$ ($i = R, I$) correspond to Woods-Saxon (WS) forms of the potentials with parameters of the real and imaginary parts V_{R}, W_{I}, R_{I}, a_{I} [$f_{\mathrm{R}}(r, R_{\mathrm{R}}, a_{\mathrm{R}})$ and $f_{\mathrm{I}}(r, R_{\mathrm{I}}, a_{\mathrm{I}})$], as they are used in the DWUCK4 code [61] and applied for numerical calculations. We determine the values of these parameters by fitting the WS potentials to the microscopically calculated potentials $V^F(r)$ and $W(r)$.

B. Results of calculations of elastic scattering cross sections

In the calculations of the microscopic OPs for the scattering of ^{10,11}Be on protons and nuclei, we used realistic density distributions of ^{10}Be calculated within the QMC model [50,51] and of ^{10,11}Be from the generator coordinate method [52]. In general, the QMC methods include both variational and Green"s function Monte Carlo methods. In our case, within the QMC method the proton and neutron densities of ^{10}Be have been computed with the AV18+IL7 Hamiltonian [51]. As far as the GCM densities are concerned, in Ref. [52] the ^{10}Be wave functions are defined in the harmonic oscillator model with all p-shell configurations. The ^{11}Be wave functions are described in terms of cluster wave functions, relative to ^{10}Be and to the external neutron. Thus, both microscopic densities effectively account for the nonordinary nuclear structure peculiarities of ^{10,11}Be [26,27] and their use is physically justified. The QMC and GCM densities are given in Fig. 1. It can be seen that they have been calculated with enough accuracy up to distances much larger than the nuclear radius. In both methods the densities of ^{10}Be occur quite similarly up to $r \sim 3.5$ fm and a difference between them is seen in their asymptotics. In the calculations of the OPs for ^{10,11}Be + ^{12}C the density of ^{12}C was taken in symmetrized Fermi form with radius and diffuseness parameters $c = 3.593$ fm and $a = 0.493$ fm, respectively [62]. The results of the calculations are compared with the available experimental data. All calculations of elastic scattering using the obtained OPs are performed by using the DWUCK4 code [61].

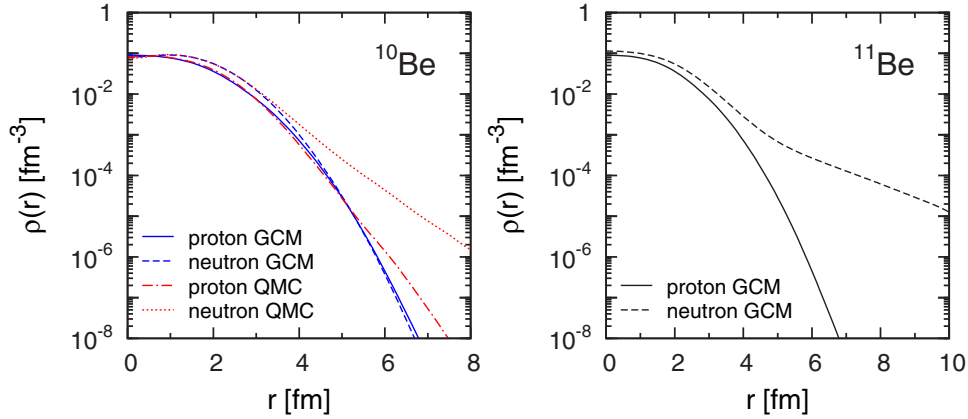

FIG. 1. (Color online) Point-proton (normalized to $Z = 4$) and point-neutron (normalized to $N = 6$ and $N = 7$, respectively) densities of ^{10}Be and ^{11}Be obtained in the GCM [52] and in the QMC method [50,51].

1. *Elastic scattering cross sections of* ^{10,11}Be + *p*

On the basis on the scheme presented in Sec. II A, we calculated the elastic scattering cross sections of $^{10,11}\mathrm{Be}+p$ and compared them with the available experimental data.

It is accepted that the elastic scattering of light nuclei is rather sensitive to their periphery, where transfer and breakup processes also take place. Therefore, investigating the elastic scattering, one must bear in mind that virtual nonelastic contributions can also take part in the process. It has been pointed out in our previous papers [42,43], as well as in Refs. [36,37,40], that the inclusion of a surface imaginary term to the OP [Eq. (1)] leads to a better agreement with the experimental data. As is known, this contribution can be considered to be the so-called dynamical polarization potential, which allows one to simulate the surface effects caused by the latter. In fact, the imaginary part of the ls term in our OP [see Eq. (1)] plays effectively this role. However, sometimes one needs to increase the absorption in the surface region and thus, one adds a derivative of the ImOP (surface term),

$$W^{\mathrm{sf}}(r) = -iN_{\mathrm{I}}^{\mathrm{sf}} r \frac{dW(r)}{dr}, \tag{5}$$

where $N_{\mathrm{I}}^{\mathrm{sf}}$ is also a fitting parameter.

The results for the elastic $^{10}\mathrm{Be}+p$ and $^{11}\mathrm{Be}+p$ scattering cross sections are given in Figs. 2 and 3, respectively, and compared with the data at energies 39.1 MeV/nucleon [63] and 59.4 MeV/nucleon [28] for ^{10}Be and 38.4 MeV/nucleon [63] and 49.3 MeV/nucleon [28] (see also Ref. [64]) for ^{11}Be. In general, our analysis points out that more successful results are obtained in the case when the ImOP is taken from HEA: $W(r) = W^{\mathrm{H}}(r)$ [Eq. (4)]. We note that in the fitting procedure of the theoretical results to the data for elastic scattering cross sections for $^{10,11}\mathrm{Be}+p$ (and also for $^{10,11}\mathrm{Be}+{}^{12}\mathrm{C}$) there arises an ambiguity in the choice of the optimal curve among many of them that is close to the experimental data. Owing to this we impose a physical constraint, namely choosing those ReOPs and ImOPs that give volume integrals that have a correct dependence on the energy. The volume integrals have the forms

$$J_V(E) = -\frac{4\pi}{A_{\mathrm{p}}A_{\mathrm{t}}}\int drr^2[N_{\mathrm{R}}V^{\mathrm{F}}(r)], \tag{6}$$

$$J_W^{(a)}(E) = -\frac{4\pi}{A_{\mathrm{p}}A_{\mathrm{t}}}\int drr^2[N_{\mathrm{I}}W(r)], \tag{7}$$

$$J_W^{(b)}(E) = -\frac{4\pi}{A_{\mathrm{p}}A_{\mathrm{t}}}\int drr^2\left[N_{\mathrm{I}}W(r) - N_{\mathrm{I}}^{\mathrm{sf}} r\frac{dW(r)}{dr}\right], \tag{8}$$

where A_{p} and A_{t} are the mass numbers of the projectile and the target, respectively. In Eq. (8) we added also the integral over the surface term of the OP (5). It is known [65] that the volume integrals (their absolute values) for the ReOP decrease with the increase of the energy, while for the ImOP they increase up to a plateau and then decrease. The values of the N parameters from the fitting procedure and after imposing the mentioned constraint are given in Table I. It can be seen that the tendency (the decrease of J_V and the increase of J_W) is generally confirmed.

The calculated differential cross sections of $^{10}\mathrm{Be}+p$ elastic scattering at energies 39.1 and 59.4 MeV/nucleon are presented in Fig. 2. First, it is seen from the top panels that the inclusion of only the volume OP is not enough to reproduce reasonably well the data in the small-angle region. Then, after adding the spin-orbit component to the OP the agreement with the data becomes better, in particular for the angular distributions calculated using the GCM density at energies 39.1 and 59.4 MeV/nucleon for angles less than 20° and 30°, correspondingly, as illustrated in the middle panels of Fig. 2. However, a discrepancy at larger angles remains. At the same time for the cross sections with the account for the ls interaction and using the QMC density we obtain fairly good agreement with the data at both energies and only a small discrepancy is seen at small angles at energy 59.4 MeV/nucleon. Further improvement is achieved when both ls- and surface terms are included in the calculations. In this case, as can be seen from the bottom panels of Fig. 2, the discrepancy between the differential cross sections for the GCM density and the experimental data at larger angles is strongly reduced.

In general, the account for the spin-orbit term in the volume OP gives a trend of an increase of the cross sections at larger angles, which seems to be related with the change of the form of the total OP at its periphery. If we evaluate the quantities of the two densities of ^{10}Be on the basis of the values of the parameter N_{R} (comparing which ones are closer to unity), our conclusion is that in the calculations without an ls interaction the GCM density works better, while in the case with an ls term in the OP the QMC density gives better results. A fair agreement between the calculated $^{10}\mathrm{Be}+p$ angular distributions and the experimental data is obtained only when both ls and surface contributions to the OP are included.

In Fig. 3 elastic cross sections for the scattering of ^{11}Be on protons at energies 38.4 and 49.3 MeV/nucleon applying the fitting procedure for the parameters N are given and compared with the empirical data. All of them are calculated using GCM density of ^{11}Be. The different curves drawn in Fig. 3 correspond to those given in Fig. 2 with accounting for different contributions to the OP. One can see a discrepancy at small angles ($\theta < 30°$) that seems to be related to the contributions from the surface region of interactions, where breakup processes play an important role. Similarly to the results for the $^{10}\mathrm{Be}+p$ elastic scattering cross sections (see Fig. 2), the account for both spin-orbit and surface terms to the OP leads to a better agreement with the $^{11}\mathrm{Be}+p$ data in the region of small angles. In Table I are given the corresponding values of the parameters N_{R} and N_{I}, whose values deviate from unity by about 20%–30%, which points out that the hybrid model for the OP can be used successfully in such calculations.

We would like to emphasize the fact that when considering the case of the total OP [Eqs. (1) and (5)], the values of the parameters N_{I} drop down sufficiently in comparison with their values coming out from the two other cases. They are compensated in most cases by the nonzero values of N_{R}^{ls}, N_{I}^{ls}, and $N_{\mathrm{I}}^{\mathrm{sf}}$ parameters. Here we would like to note that the ls term used in our calculations (with both real and imaginary parts) plays a similar role as the surface term applied in Ref. [37], where, however, the imaginary ls term is disregarded. From our analysis made for the elastic scattering of ^{10}Be and ^{11}Be on protons, we conclude also that the surface imaginary part of the

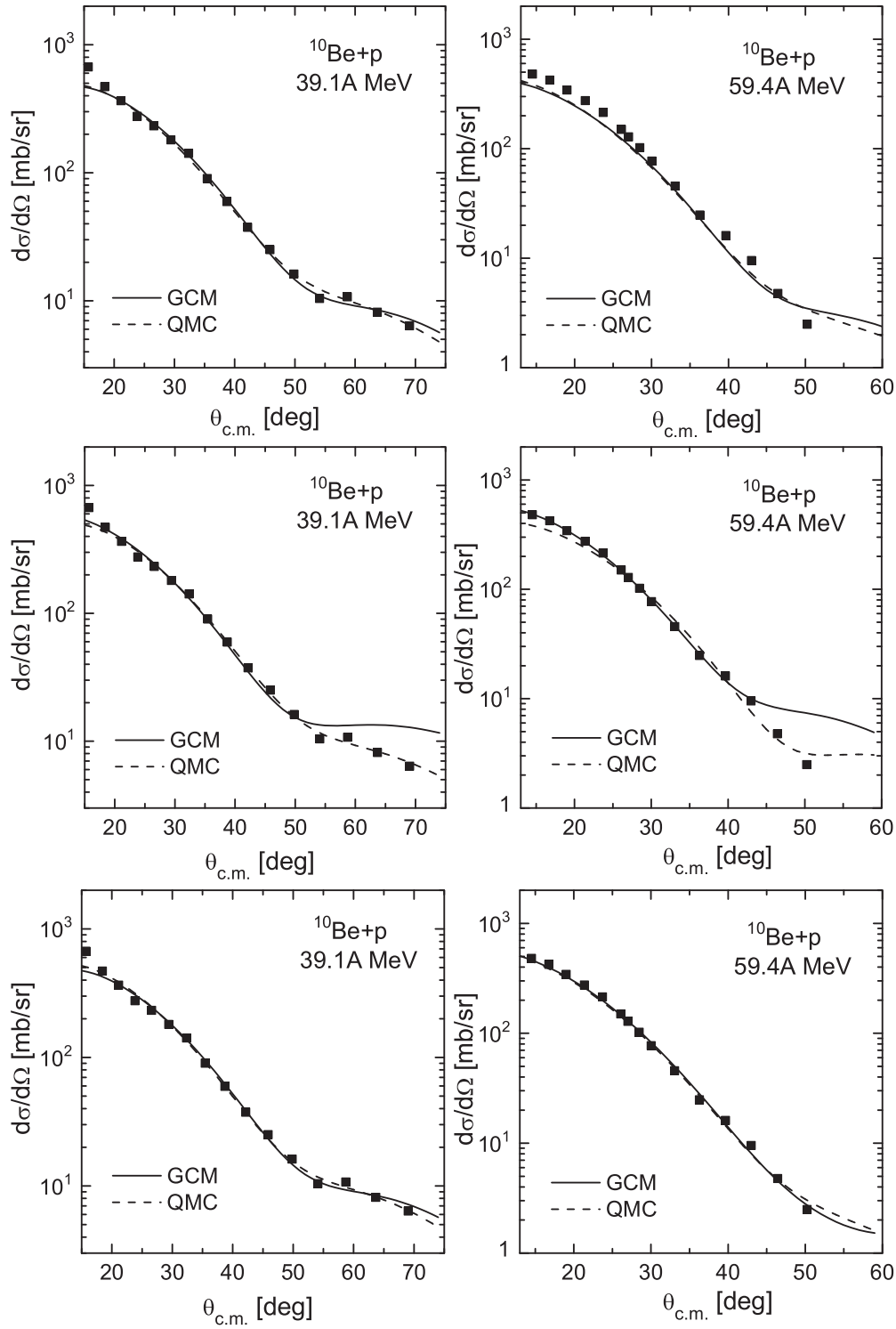

FIG. 2. ^{10}Be + p elastic scattering cross sections. (Top) Without ls term; (middle) with ls term; (bottom) with both ls and surface terms. Solid lines: calculations with GCM density of ^{10}Be; dashed lines: calculations with QMC density of ^{10}Be. Experimental data for 39.1 MeV/nucleon and 59.4 MeV/nucleon are taken from Refs. [63] and [28], respectively.

OP is less necessary to fit the data of proton elastic scattering on the stable nucleus ^{10}Be, but it is important to have an agreement with the proton elastic-scattering data of the halo nucleus ^{11}Be. This is mainly attributable to the specific halo structure of the ^{11}Be density distribution and its large rms radius.

For a more complete analysis of the elastic scattering cross sections, we extend the incident energy region to lower energies in the example of the scattering of ^{10}Be on protons that has been recently studied by Schmitt *et al.* [66]. Moreover, this could be a test of our hybrid model at low energies. In

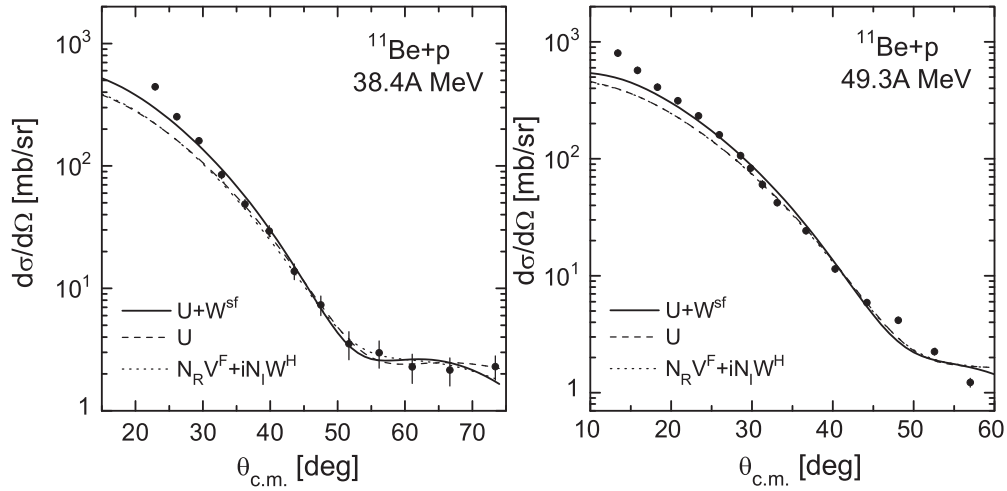

FIG. 3. ^{11}Be + p elastic scattering cross sections. Calculations are performed with GCM density of ^{11}Be. Solid line, OP with both ls and surface terms [Eqs. (1) and (5)]; dashed line, OP with ls term [Eq. (1)]; dotted line, the volume part of OP from Eq. (1). Experimental data for 38.4 and 49.3 MeV/nucleon are taken from Refs. [63] and [28], respectively.

Ref. [66] proton energies of 6, 7.5, 9, and 10.7 MeV were selected to measure the elastic scattering cross sections for protons with ^{10}Be beams in inverse kinematics to provide constraints on optical potentials for reaction studies with light neutron-rich nuclei. The calculated results for the differential cross sections, shown as a ratio to Rutherford scattering, are given and compared with the data [66] in Fig. 4 for energies of 7.5 and 10.7 MeV. The values of the N parameters from the fitting procedure and the corresponding total reaction cross sections and volume integrals are listed in Table II. The results shown in Fig. 4 when including in the calculations only the ls term demonstrate a fairly good agreement with the data. The values of the parameters N_R deduced from the fitting procedure for both energies in the case of GCM density of ^{10}Be are quite large, which indicates the specific peculiarities of the elastic scattering at low energies, accounting for the spin-orbit term. We also calculated the ^{10}Be + p elastic scattering cross sections at the same proton energies, taking into account the

TABLE I. The renormalization parameters N_R, N_I, N_R^{ls}, N_I^{ls}, and N_I^{sf}, the total reaction cross sections σ_R (in mb), and the volume integrals J_V, $J_W^{(a)}$, and $J_W^{(b)}$ (in MeV.fm^3) as functions of the energy E = 39.1 and 59.4 MeV/nucleon for the ^{10}Be + p and E = 38.4 and 49.3 MeV/nucleon for the ^{11}Be + p elastic scattering.

Nucleus	Model	E	N_R	N_I	N_R^{ls}	N_I^{ls}	N_I^{sf}	σ_R	J_V	$J_W^{(a)}$	$J_W^{(b)}$
^{10}Be	GCM	39.1	0.983	0.267	0.000	0.000	0.000	292.12	389.408	116.600	116.600
without ls and	QMC		1.153	0.295	0.000	0.000	0.000	311.36	411.344	130.806	130.806
surface terms	GCM	59.4	1.001	0.802	0.000	0.000	0.000	341.18	333.739	263.540	263.540
	QMC		1.188	0.856	0.000	0.000	0.000	356.98	354.606	283.464	283.464
^{10}Be	GCM	39.1	1.493	0.492	1.000	0.476	0.000	372.50	591.440	216.480	216.480
with ls and	QMC		1.163	0.318	0.557	0.000	0.000	323.96	414.911	141.004	141.004
without surface	GCM	59.4	1.294	0.804	0.190	0.000	0.000	355.29	431.427	264.197	264.197
terms	QMC		1.014	0.527	0.940	0.000	0.000	287.68	302.669	174.516	174.516
^{10}Be	GCM	39.1	0.995	0.266	0.095	0.082	0.004	298.65	394.161	117.040	122.321
with ls and	QMC		1.194	0.260	0.075	0.025	0.018	333.71	425.971	115.286	139.235
surface terms	GCM	59.4	0.970	0.000	0.365	1.000	0.373	400.26	323.404	0.000	367.802
	QMC		1.043	0.281	0.000	1.000	0.270	389.27	311.325	93.053	361.343
^{11}Be	GCM	38.4	0.824	0.659	0.000	0.000	0.000	459.05	339.388	293.493	293.493
without ls and		49.3	0.793	0.805	0.000	0.000	0.000	423.52	296.301	301.184	301.184
surface terms											
^{11}Be	GCM	38.4	0.787	0.799	0.000	0.507	0.000	458.63	324.148	355.844	355.844
with ls and		49.3	0.793	0.867	0.123	0.316	0.000	426.85	296.301	301.184	301.184
without surface											
terms											
^{11}Be with	GCM	38.4	0.849	0.106	0.102	0.380	0.152	493.01	349.685	47.208	269.903
ls and surface		49.3	0.801	0.000	0.213	0.394	0.200	436.46	299.280	0.000	246.162
terms											

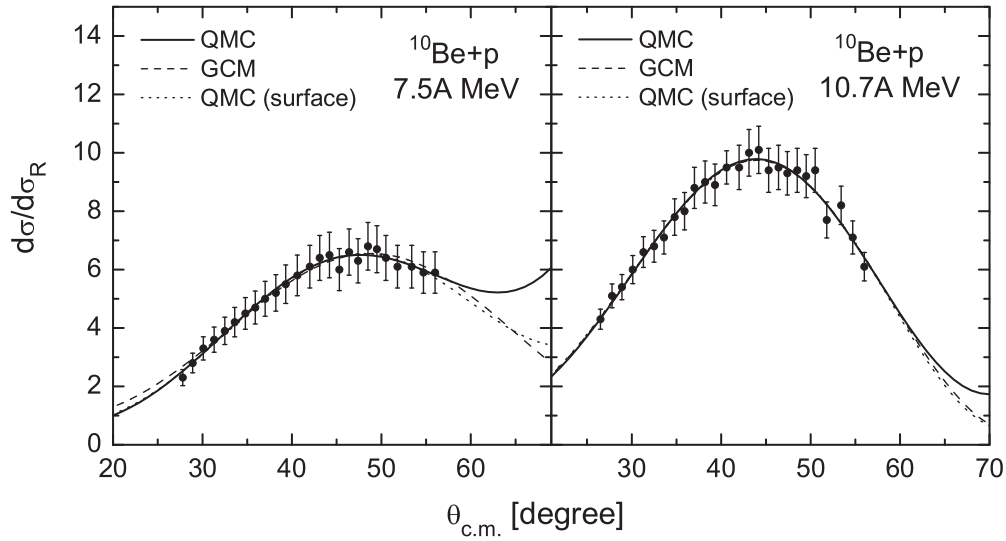

FIG. 4. ^{10}Be + p elastic scattering cross sections as a ratio to Rutherford scattering at proton energies of 7.5 MeV (left) and 10.7 MeV (right). The solid and dashed lines show the results with QMC and GCM density of ^{10}Be, respectively, and with ls term in OP. The dotted lines show the QMC results obtained by accounting for both the ls and surface terms in OP. Experimental data are taken from Ref. [66].

surface term [Eq. (5)]. In this case, only the QMC density of ^{10}Be was tested, which has been also used in Ref. [37], where the two other energies of 6 and 9 MeV were considered. The results illustrate that the inclusion of the surface contribution does not affect the good agreement obtained without it. Here we note that in Ref. [66] no single optical potential had been found to reproduce well the proton elastic scattering data over this range of energies. At the same time, a deviation of the results of our model with both densities beyond 55° is seen from the left panel of Fig. 4. Therefore, it would be desirable to measure the elastic channel in this angular range to constrain the $p-^{10}$ Be optical potential.

2. *Elastic scattering cross sections of* ^{10,11}Be + ^{12}C

The elastic scattering cross sections of ^{10,11}Be + ^{12}C (their ratios to the Rutherford one) calculated within the hybrid model at the same energies as for ^{10,11}Be + p scattering are given in Figs. 5 and 6 and compared with the experimental data (see also Ref. [64]). In comparison with the case of ^{10,11}Be + p, the experimental data [28,63] for the scattering on ^{12}C demonstrate more developed diffractional picture on the basis of the stronger influence of the Coulomb field. It can be seen in Fig. 5 that in both cases of calculations of OPs with QMC or GCM densities the results are in a good agreement with the available data. It is seen also from the figures that it is difficult to determine the advantage of the use for the ImOP $W = W^{\rm H}$ or $W = V^{\rm F}$, because the differences between the theoretical results start at angles for which the experimental data are not available. The values of the parameters $N_{\rm R}$ and $N_{\rm I}$ (the depths of ReOP and ImOP) are given in Table III. From the comparison of these values, when GCM or QMC densities are used, one can see that in the case of GCM densities the values of the parameters are closer to unity. In this way, we may conclude that, as in the ^{10}Be + p case without ls term of OP, the GCM density can be considered as a more realistic one.

III. BREAKUP REACTIONS OF ^{11}Be

A. The ^{10}Be + n model of ^{11}Be

In this section we consider the characteristics of breakup processes of the ^{11}Be nucleus, namely diffraction and stripping reaction cross sections and the momentum distributions of the fragments. We use a simple model in which ^{11}Be consists of a core of ^{10}Be and a halo of a single neutron (see, e.g., Ref. [54]). In this model the density of ^{10}Be has to be given. As in Sec. II we use the QMC [50] and GCM [52] density distributions of ^{10}Be. The hybrid model is applied to calculate the OP of

TABLE II. The renormalization parameters $N_{\rm R}$, $N_{\rm I}$, $N_{\rm R}^{ls}$, $N_{\rm I}^{ls}$, and $N_{\rm I}^{\rm sf}$, the total reaction cross sections $\sigma_{\rm R}$ (in mb), and the volume integrals J_V, $J_W^{(a)}$, and $J_W^{(b)}$ (in MeV fm^3) as functions of the proton energy $E = 7.5$ and 10.7 MeV for the ^{10}Be + p elastic scattering.

Nucleus	Model	E	$N_{\rm R}$	$N_{\rm I}$	$N_{\rm R}^{ls}$	$N_{\rm I}^{ls}$	$N_{\rm I}^{\rm sf}$	$\sigma_{\rm R}$	J_V	$J_W^{(a)}$	$J_W^{(b)}$
^{10}Be	GCM	7.5	2.287	0.473	0.000	0.425	0.000	906.19	1215.283	527.749	527.749
with ls and	QMC		1.244	0.056	0.065	0.103	0.000	330.03	603.634	62.966	62.966
without surface	GCM	10.7	2.232	1.129	0.000	0.759	0.000	804.23	1144.742	1151.009	1151.009
terms	QMC		1.915	0.247	0.963	0.307	0.000	722.54	895.179	253.766	253.766
^{10}Be	QMC	7.5	1.483	0.000	0.442	0.208	0.044	306.28	719.605	0.000	148.453
with ls and	QMC	10.7	1.354	0.098	0.178	1.000	0.193	636.50	632.936	100.685	695.676
surface terms											

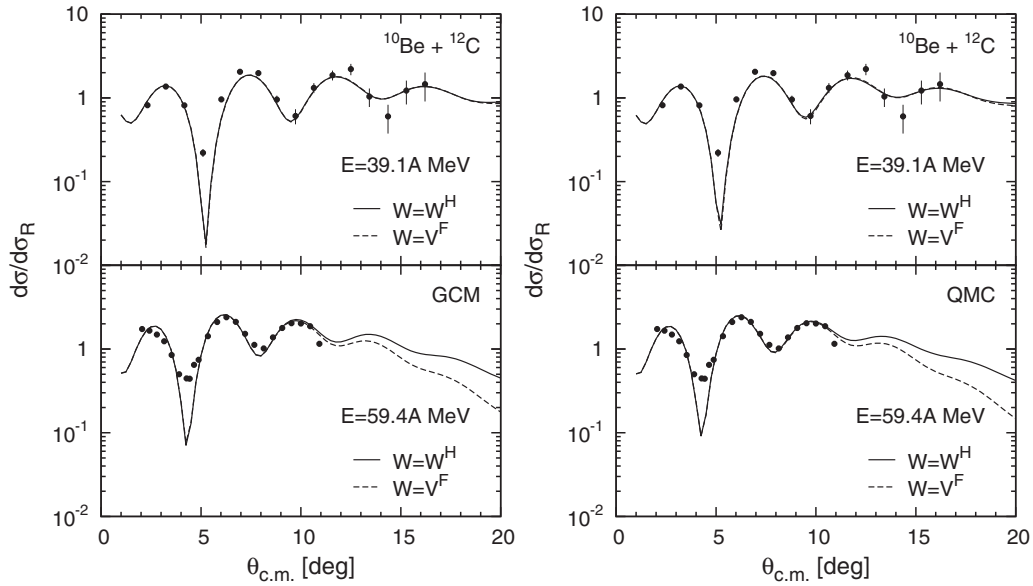

FIG. 5. ^{10}Be + ^{12}C elastic scattering cross sections. Solid lines, $W = W^H$; dashed lines, $W = V^F$. (Left) Calculations with GCM density of ^{10}Be; (right) calculations with QMC density of ^{10}Be. Experimental data for 39.1 and 59.4 MeV/nucleon are taken from Refs. [63] and [28], respectively.

the interaction of ^{10}Be with the target, as well as OP for the n + target interaction. In the final step of the procedure the sum of these potentials is folded with the respective density distribution corresponding to the relative motion wave function of the clusters in ^{11}Be. The latter is obtained by solving the Schrödinger equation with the WS potential for a particle with a reduced mass of two clusters. The parameters of the WS potentials are obtained by a fitting procedure, namely, to reach the neutron separation energy $S_n = 504 \pm 6$ KeV. They have the following values for $2s$ state in which the valence neutron in ^{11}Be is mainly bound (see Refs. [16,67]): $R = 2.7$ fm, $a = 0.52$ fm, and $V_0 = 61$ MeV. The rms radius of the cluster formation is obtained to be 6.87 fm.

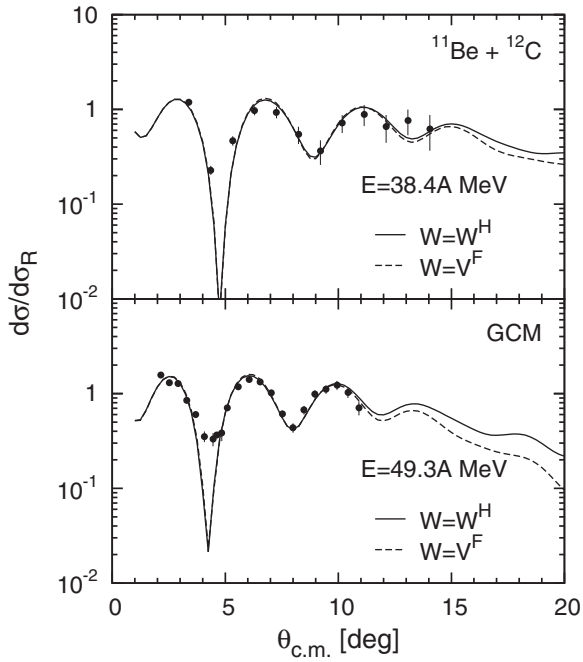

FIG. 6. ^{11}Be + ^{12}C elastic scattering cross sections. Solid lines, $W = W^{\mathrm{H}}$; dashed lines, $W = V^{\mathrm{F}}$. For ^{11}Be GCM density was used. Experimental data for 38.4 and 49.3 MeV/nucleon are taken from Refs. [63] and [28], respectively,

The s state ($l = 0$, $n = 1,2$) of the relative motion of two clusters has the form

$$\phi_{00}^{(n)}(\mathbf{s}) = \phi_0^{(n)}(s)\frac{1}{\sqrt{4\pi}}, \quad n = 1,2. \tag{9}$$

The corresponding density distribution is the probability of both clusters to be at a mutual distance s:

$$\rho_0^{(n)}(\mathbf{s}) = \left|\phi_{00}^{(n)}(\mathbf{s})\right|^2 = \frac{1}{4\pi}\left|\phi_0^{(n)}(s)\right|^2. \tag{10}$$

Within the ^{10}Be + n cluster model, to calculate the ^{11}Be breakup in its collision with the protons and nuclear targets, one should calculate two OPs of ^{10}Be + p (or A) and n + p (or A) scattering:

$$\begin{aligned} U^{(b,n)}(r) &= V^{(b,n)} + iW^{(b,n)} \\ &= \int d\mathbf{s}\rho_0^{(n)}(s)\left\{U_c^{(n)}[\mathbf{r} + (1/11)\mathbf{s}]\right. \\ &\quad \left. + U_n^{(n)}[\mathbf{r} - (10/11)\mathbf{s}]\right\} \\ &= 2\pi\int_0^\infty \rho_0^{(n)}(s)s^2 ds \\ &\quad \times \int_{-1}^{1} dx\left\{U_c^{(n)}[\sqrt{r^2 + (1s/11)^2 + r(2/11)sx}]\right. \\ &\quad \left. + U_n^{(n)}[\sqrt{r^2 + (10s/11)^2 - r(20/11)sx}]\right\}. \end{aligned} \tag{11}$$

In Eq. (11) $\mathbf{r} - (10/11)\mathbf{s} \equiv \mathbf{r}_n$ and $\mathbf{r} + (1/11)\mathbf{s} \equiv \mathbf{r}_c$ give the distances between the centers of each of the clusters and

TABLE III. The renormalization parameters N_R and N_I, the total reaction cross sections σ_R (in mb), and the volume integrals J_V and J_W (in MeV fm^3) as functions of the energy $E = 39.1$ and 59.4 MeV/nucleon for the ^{10}Be + ^{12}C and $E = 38.4$ and 49.3 MeV/nucleon for the ^{11}Be + ^{12}C elastic scattering.

Nucleus	Model	E	W	N_R	N_I	σ_R	J_V	$J_W^{(a)}$
^{10}Be	GCM	39.1	W^H	0.939	0.708	104.539	255.156	283.037
			V^F	0.816	0.465	105.958	221.733	126.355
		59.4	W^H	1.013	1.010	101.052	238.122	302.581
			V^F	0.884	0.577	102.635	207.798	135.633
^{10}Be	QMC	39.1	W^H	0.888	0.620	105.332	245.613	249.769
			V^F	0.782	0.434	106.878	216.294	120.041
		59.4	W^H	0.970	0.887	101.616	231.953	267.782
			V^F	0.849	0.534	103.035	203.019	127.694
^{11}Be	GCM	38.4	W^H	0.769	0.711	127.123	216.879	287.235
			V^F	0.708	0.521	126.825	199.676	146.937
		49.3	W^H	0.820	0.883	124.406	213.754	300.193
			V^F	0.743	0.574	123.302	193.682	149.628

the target, and $\mathbf{s} = \mathbf{s}_1 + \mathbf{s}_2 = (10/11)\mathbf{s} + (1/11)\mathbf{s}$ determines the relative distance between the centers of the two clusters. s_1 and s_2 are the distances between the centers of ^{11}Be and each of the clusters, correspondingly. The respective OPs for the ^{10}Be + A and $n + A$ scattering are calculated within the microscopic model of OP from Sec. II A.

In the case of the ^{11}Be breakup on the proton target, the $n + p$ potential is taken in the form [68] (in MeV)

$$U_n^{(n)} = v_{np} = v(r)(1 + i\gamma), \tag{12}$$

with

$$v(r) = 120e^{-1.487r^2} - 53.4e^{-0.639r^2} - 27.55e^{-0.465r^2}, \tag{13}$$

where $\gamma = 0.4$.

For calculations of breakup cross sections and momentum distributions of fragments in the ^{10}Be + n breakup model we give here briefly the eikonal formalism, namely the expressions of the S matrix (as a function of the impact parameter b),

$$S(b) = \exp\left[-\frac{i}{\hbar v}\int_{-\infty}^{\infty} U(\sqrt{b^2 + z^2})dz\right], \tag{14}$$

where

$$U = V + iW \tag{15}$$

is the OP. For negative V and W one can write

$$S(b) = \left[\cos\left(\frac{1}{\hbar v}\int_{-\infty}^{\infty}|V|dz\right) + i\sin\left(\frac{1}{\hbar v}\int_{-\infty}^{\infty}|V|dz\right)\right] \times \exp\left[-\frac{1}{\hbar v}\int_{-\infty}^{\infty}|W|dz\right], \tag{16}$$

and, correspondingly,

$$|S(b)| = \exp\left[-\frac{1}{\hbar v}\int_{-\infty}^{\infty}|W|dz\right]. \tag{17}$$

In our case W is the imaginary part of the microscopic OP [Eq. (11)]. $|S(b)|^2$ gives the probability that after the collision with a proton ($z \to \infty$) (in the ^{11}Be + p scattering), the cluster c or the neutron with impact parameter b remains in the elastic channel ($i = c,n$):

$$|S_i(b)|^2 = \exp\left[-\frac{2}{\hbar v}\int_{-\infty}^{\infty} dz\left|W_I(\sqrt{b^2 + z^2})\right|\right]. \tag{18}$$

The probability of a cluster being removed from the elastic channel is $(1 - |S|^2)$. The probability of the case when both clusters (c and n) leave the elastic channel is $(1 - |S_n|^2)(1 - |S_c|^2)$. As shown in the next section, Eqs. (14)–(18) take part in the calculations of the diffraction breakup and stripping reaction cross sections.

B. Momentum distributions of fragments

The necessary quantity to calculate the diffraction breakup and absorption scattering cross sections (differential and total) and momentum distributions is the probability function of the **k**-momentum distribution of a cluster in the system of two clusters as a function of the impact parameter **b** [16]:

$$\frac{d^3P_\Omega(\mathbf{b},\mathbf{k})}{d\mathbf{k}} = \frac{1}{(2\pi)^3}\left|\int d\mathbf{s}\phi_{\mathbf{k}}^*(\mathbf{s})\Omega(\mathbf{b},\mathbf{r}_\perp)\phi_{00}^{(n)}(\mathbf{s})\right|^2. \tag{19}$$

In Eq. (19) $\Omega(\mathbf{b},\mathbf{r}_\perp)$ is given by the products of two S functions S_c and S_n [Eqs. (14)–(18)] of the core ^{10}Be and the neutron, $\phi_{\mathbf{k}}(\mathbf{s})$ is the continuum wave function, **k** is the relative momentum of both clusters in their center-of-mass frame, and the vector $\mathbf{r}_\perp$ is the projection of the relative coordinate **s** between the centers of the two clusters on the plane normal to the z axis. The bound-state wave function ϕ_{00} of the relative motion of two clusters is given for the s state by Eq. (9). As to the wave function in the final state $\phi_{\mathbf{k}}$, we neglect its distortion and, thus, replace it with $j_0(ks)$ in the case of the s state. Then, following Ref. [16], the probability function has the form

$$\frac{d^2P_\Omega(\mathbf{b},\mathbf{k})}{dk_L dk_\perp} = \frac{k_\perp}{16\pi^3k^2}\left|\int ds\int d(\cos\theta_s)\,g(s)\sin(ks) \times \int d\varphi_s\Omega(\mathbf{b},\mathbf{r}_\perp)\right|^2, \tag{20}$$

where

$$\Omega(\mathbf{b},\mathbf{r}_\perp) = S_c(\mathbf{b}_c)S_n(\mathbf{b}_n) \tag{21}$$

and $g(s) = s\phi_0^{(n)}(s)$, $\phi_0^{(n)}$ being given by Eq. (9).

Hence, the diffraction breakup cross section has the form

$$\left(\frac{d\sigma}{dk_L}\right)_{\rm diff} = \int_0^\infty b_n db_n \int_0^{2\pi} d\varphi_n \int_0^\infty dk_\perp \frac{d^2P_\Omega(\mathbf{k},\mathbf{b})}{dk_L dk_\perp}. \tag{22}$$

In Eq. (22) $d^2P_\Omega(\mathbf{b},\mathbf{k})/dk_L dk_\perp$ is given by Eq. (20). The integrals over b_n and φ_n mean integration over the impact parameter $\mathbf{b}_n$ of the neutron with respect to the target.

The cross sections of the stripping reaction when the neutron leaves the elastic channel is [16]

$$\left(\frac{d\sigma}{dk_L}\right)_{\rm str} = \frac{1}{2\pi^2}\int_0^\infty b_n d\, b_n d\varphi_n [1-|S_n(b_n)|^2] \times \int \rho d\rho d\varphi_\rho |S_c(b_c)|^2 \times \left[\int_0^\infty dz \cos(k_L z)\phi_0(\sqrt{\rho^2+z^2})\right]^2. \tag{23}$$

Equation (23) is obtained when the incident nucleus has spin equal to zero and for the s state of the relative motion of two clusters in the nucleus with $\mathbf{s} = \mathbf{r}_c - \mathbf{r}_n$, $\rho = \mathbf{b}_c - \mathbf{b}_n$, $\mathbf{s} = \rho + \mathbf{z}$, and

$$b_c = \sqrt{s^2\sin^2\theta + b_n^2 + 2sb_n\sin\theta\cos(\varphi-\varphi_n)} \tag{24}$$

coming from $\mathbf{b}_c = \mathbf{b}_n + \mathbf{b}$, where $b = s\sin\theta$ is the projection of $\mathbf{s}$ on the plane normal to the z axis along the straight-line trajectory of the incident nucleus.

In the end of this section we note that the real and imaginary parts of the OPs taking part in Eq. (11) and in the S matrices [Eqs. (14)–(18)] are used for calculations of the cross sections [Eqs. (19)–(24)] in the cases of scattering and breakup of ^{11}Be on protons and nuclei that will be considered in the following part of our work. They are calculated microscopically within the hybrid model given in Sec. II A.

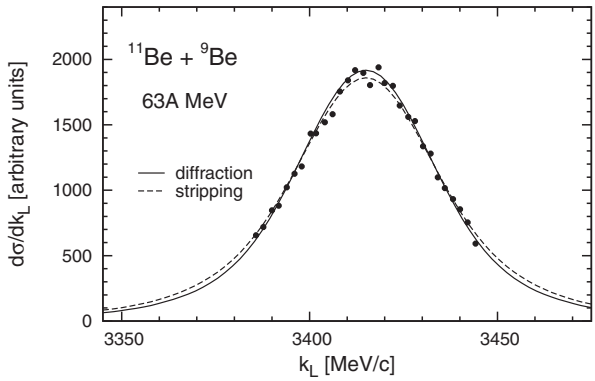

FIG. 7. Cross sections of diffraction breakup and stripping reaction in ^{11}Be + ^{9}Be scattering at $E = 63$ MeV/nucleon. Experimental data are taken from Ref. [13].

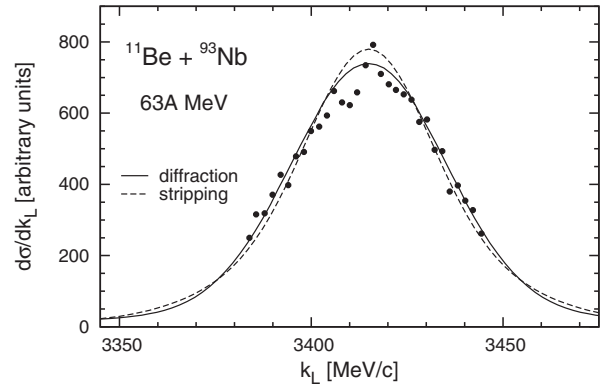

FIG. 8. The same as Fig. 7, but for ^{11}Be + ^{93}Nb scattering.

C. Results of calculations of breakup reactions

In this section we perform calculations of the breakup cross sections of ^{11}Be on the target nucleus ^{9}Be and heavy nuclei, such as ^{93}Nb, ^{181}Ta, and ^{238}U, and compare our results with the available experimental data [13]. The densities of these heavy nuclei needed to compute the OPs are taken from Ref. [69]. The diffraction and stripping cross sections (when a neutron leaves the elastic channel) for reactions ^{11}Be + ^{9}Be, ^{11}Be + ^{93}Nb, ^{11}Be + ^{181}Ta, and ^{11}Be + ^{238}U are calculated from Eqs. (22) and (23). The obtained results are illustrated in Figs. 7, 8, 9, and 10, respectively. We note the good agreement with the experimental data from light and heavy breakup targets. The obtained cross sections for the diffraction and stripping have a similar shape. The values of the widths are around 50 MeV, in agreement with the experimental ones. Our results confirm the observations (e.g., in Refs. [11,12]) that the width almost does not depend on the mass of the target and, as a result, it gives information basically about the momentum distributions of two clusters. Here we note that owing to the arbitrary units of the measured cross sections of the considered processes it was not necessary to renormalize the depths of our OPs of the fragment-target nuclei interactions.

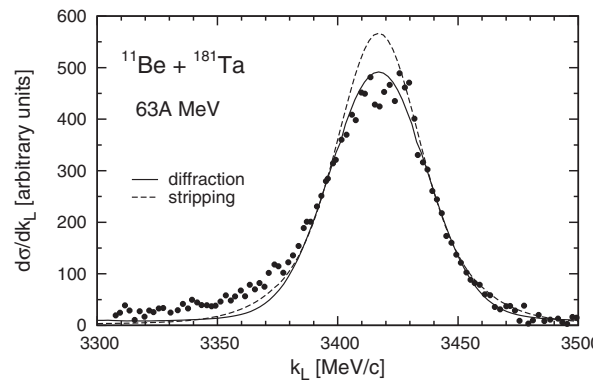

FIG. 9. The same as Fig. 7, but for ^{11}Be + ^{181}Ta scattering.

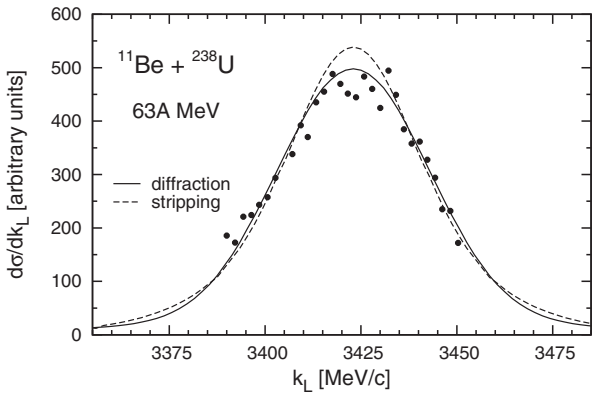

FIG. 10. The same as Fig. 7, but for ^{11}Be + ^{238}U scattering.

IV. CONCLUSIONS

In the present work the hybrid model is applied to study characteristics of the processes of scattering and reactions of ^{10}Be and ^{11}Be on protons and nuclei. In the model, the ReOP is calculated microscopically in a folding procedure of the densities of the projectile and the target with effective NN interactions related to the g matrix obtained on the basis of the Paris NN potential. The ReOP includes both the direct and the exchange terms. The ImOP is calculated microscopically as the folding OP that reproduces the phase of scattering obtained in the high-energy approximation. The only free parameters in the hybrid model (N) are the coefficients that correct the depths of the ReOP, ImOP, and the spin-orbit parts of OP. Their values are obtained by a fitting procedure to the experimental data whenever they exist. Additionally, in some cases the surface absorption is accounted for by including another term to the OP that requires one more fitting parameter. The density distributions of ^{10}Be obtained within GCM and QMC microscopic methods and of ^{11}Be from GCM are used. The OPs resulting within the hybrid model are applied to calculate characteristics of various processes.

The results of the present work can be summarized as follows.

(i) Elastic scattering cross sections of ^{10}Be and ^{11}Be on protons and ^{12}C are calculated using the microscopic OPs for energies $E < 100$ MeV/nucleon and compared with the existing experimental data. To resolve the ambiguities of the magnitudes of the depths of the OPs, the well-established energy dependence of the respective volume integrals of the OPs is taken into account. The theoretical approach gives a good explanation of a wide range of empirical data on the ^{10,11}Be + p and ^{10,11}Be + ^{12}C elastic scattering. It was established that the values of the coefficients N_R (depths of ReOP) obtained by fitting procedure are close to unity. The correction of the ImOP by factor N_I is in some cases larger, e.g., for ^{10}Be + p at energy $E = 39.1$ MeV/nucleon in the case when the spin-orbit (ls) component is not accounted for. The inclusion of a surface term to the OP leads to a better agreement with the experimental elastic scattering cross-section data. We conclude that, in general, the hybrid model for microscopic calculations of the OPs gives the basic important features of the scattering cross sections and can be recommended and applied to calculate more complex processes such as breakup reactions, momentum distributions of fragments, and others.

(ii) Apart from the usual folding model, we use another folding approach to consider the ^{11}Be breakup by means of the simple ^{10}Be + n cluster model for the structure of ^{11}Be. Within this folding model we construct the OP of the interaction of ^{10}Be with the target, as well as the n + target interaction. Using the cluster OPs ^{10}Be + p (or A) and n + p (or A) the corresponding functions S_c and S_n (S matrices) for the core and neutron within the eikonal formalism are obtained.

(iii) The calculated S_c and S_n functions are used to get results for the longitudinal momentum distributions of ^{10}Be fragments produced in the breakup of ^{11}Be on different targets. This includes the breakup reactions of ^{11}Be on ^{9}Be, ^{93}Nb, ^{181}Ta, and ^{238}U at $E = 63$ MeV/nucleon, for which a good agreement of our calculations for the diffraction and stripping reaction cross sections with the available experimental data exist. The obtained widths of about 50 MeV/c are close to the empirical ones. Future measurements of such reactions are highly desirable for the studies of the exotic ^{11}Be structure. The accurate interpretation of the expected data requires more refined theoretical approaches, for instance, that of Ref. [70] within the CDCC method and its extensions to study the effects of the dynamic core excitation, especially its large contribution to nuclear breakup in the scattering of halo nuclei.

ACKNOWLEDGMENTS

The authors are grateful to S. C. Pieper for providing with the density distributions of ^{9,10}Be nuclei calculated within the QMC method. The work is partly supported by the Project from the Agreement for Cooperation between the INRNE-BAS (Sofia) and JINR (Dubna). Four of the authors (D.N.K., A.N.A., M.K.G., and K.S.) are grateful for the support of the Bulgarian Science Fund under Contract No. DFNI–T02/19 and one of them (D.N.K.) under Contract No. DFNI–E02/6. The authors V.K.L., E.V.Z., and K.V.L. thank the Russian Foundation for Basic Research (Grant No. 13-01-00060) for partial support. K.S. acknowledges the support of the Project No. BG-051P0001-3306-003.

[1] I. Tanihata, H. Hamagaki, O. Hashimoto, S. Nagamiya, Y. Shida, N. Yoshikawa, O. Yamakawa, K. Sugimoto, T. Kobayashi, D. E. Greiner, N. Takahashi, and Y. Nojiri, Phys. Lett. B **160**, 380 (1985).

[2] I. Tanihata, H. Hamagaki, O. Hashimoto, Y. Shida, N. Yoshikawa, K. Sugimoto, O. Yamakawa, T. Kobayashi, and N. Takahashi, Phys. Rev. Lett. **55**, 2676 (1985).

[3] I. Tanihata, T. Kobayashi, O. Yamakawa, T. Shimoura, K. Ekuni, K. Sugimoto, N. Takahashi, T. Shimoda, and H. Sato, Phys. Lett. B **206**, 592 (1988).

[4] W. Mittig, J. M. Chouvel, Z. W. Long, L. Bianchi, A. Cunsolo, B. Fernandez, A. Foti, J. Gastebois, A. Gillibert, C. Gregoire, Y. Schutz, and C. Stephan, Phys. Rev. Lett. **59**, 1889 (1987).

[5] I. Tanihata, Prog. Nucl. Phys. **35**, 505 (1995), and references therein.

[6] P. G. Hansen, A. S. Jensen, and B. Jonson, Annu. Rev. Nucl. Sci. **45**, 591 (1995), and references therein.

[7] T. Kobayashi, O. Yamakawa, K. Omata, K. Sugimoto, T. Shimoda, N. Takahashi, and I. Tanihata, Phys. Rev. Lett. **60**, 2599 (1988).

[8] G. F. Bertsch, B. A. Brown, and H. Sagawa, Phys. Rev. C **39**, 1154 (1989); T. Hoshino, H. Sagawa, and A. Arima, Nucl. Phys. A **506**, 271 (1990); L. Johannsen, A. S. Jensen, and P. G. Hansen, Phys. Lett. B **244**, 357 (1990); A. C. Hayes, *ibid.* **254**, 15 (1991); G. F. Bertsch and H. Esbensen, Ann. Phys. **209**, 327 (1991); Y. Tosaka and Y. Suzuki, Nucl. Phys. A **512**, 46 (1990).

[9] R. Anne *et al.*, Phys. Lett. B **250**, 19 (1990).

[10] H. Esbensen, Phys. Rev. C **44**, 440 (1991).

[11] N. A. Orr, N. Anantaraman, S. M. Austin, C. A. Bertulani, K. Hanold, J. H. Kelley, D. J. Morrissey, B. M. Sherrill, G. A. Souliotis, M. Thoennessen, J. S. Winfield, and J. A. Winger, Phys. Rev. Lett. **69**, 2050 (1992).

[12] N. A. Orr, N. Anantaraman, S. M. Austin, C. A. Bertulani, K. Hanold, J. H. Kelley, R. A. Kryger, D. J. Morrissey, B. M. Sherrill, G. A. Souliotis, M. Steiner, M. Thoennessen, J. S. Winfield, J. A. Winger, and B. M. Young, Phys. Rev. C **51**, 3116 (1995).

[13] J. H. Kelley, S. M. Austin, R. A. Kryger, D. J. Morrisey, N. A. Orr, B. M. Sherill, M. Thoennessen, J. S. Winfield, J. A. Winger, and B. M. Young, Phys. Rev. Lett. **74**, 30 (1995).

[14] D. Baye and P. Capel, Lect. Notes Phys. **848**, 121 (2012).

[15] F. Barranco, E. Vigezzi, and R. A. Broglia, Z. Phys. A **356**, 45 (1996).

[16] K. Hencken, G. Bertsch, and H. Esbensen, Phys. Rev. C **54**, 3043 (1996).

[17] C. A. Bertulani and P. G. Hansen, Phys. Rev. C **70**, 034609 (2004).

[18] C. A. Bertulani and K. W. McVoy, Phys. Rev. C **46**, 2638 (1992).

[19] S. N. Ershov, B. V. Danilin, J. S. Vaagen, A. A. Korsheninnikov, and I. J. Thompson, Phys. Rev. C **70**, 054608 (2004).

[20] C. A. Bertulani, M. Hussein, and G. Muenzenberg, *Physics of Radioactive Beams* (Nova Science, Hauppage, NY, 2002).

[21] W. Nörtershäuser *et al.*, Phys. Rev. Lett. **102**, 062503 (2009).

[22] I. Talmi and I. Unna, Phys. Rev. Lett. **4**, 469 (1960).

[23] D. E. Alburger, C. Chasman, K. W. Jones, J. W. Olness, and R. A. Ristinen, Phys. Rev. **136**, B916 (1964).

[24] D. J. Millener, J. W. Olness, E. K. Warburton, and S. S. Hanna, Phys. Rev. C **28**, 497 (1983).

[25] J. H. Kelley, E. Kwan, J. E. Purcell, C. G. Sheu, and H. R. Weller, Nucl. Phys. A **880**, 88 (2012).

[26] A. Shrivastava *et al.*, Phys. Lett. B **596**, 54 (2004).

[27] R. Crespo, A. Deltuva, and A. M. Moro, Phys. Rev. C **83**, 044622 (2011).

[28] M. D. Cortina-Gil *et al.*, Phys. Lett. B **401**, 9 (1997); Nucl. Phys. A **616**, 215c (1997).

[29] K. Amos, W. A. Richter, S. Karataglidis, and B. A. Brown, Phys. Rev. Lett. **96**, 032503 (2006); P. K. Deb, B. C. Clark, S. Hama, K. Amos, S. Karataglidis, and E. D. Cooper, Phys. Rev. C **72**, 014608 (2005).

[30] G. R. Satchler and W. G. Love, Phys. Rep. **55**, 183 (1979); G. R. Satchler, *Direct Nuclear Reactions* (Clarendon Press, Oxford, UK, 1983).

[31] D. T. Khoa and W. von Oertzen, Phys. Lett. B **304**, 8 (1993); **342**, 6 (1995); D. T. Khoa, W. von Oertzen, and H. G. Bohlen, Phys. Rev. C **49**, 1652 (1994); D. T. Khoa, W. von Oertzen, and A. A. Ogloblin, Nucl. Phys. A **602**, 98 (1996); D. T. Khoa and H. S. Than, Phys. Rev. C **71**, 044601 (2005); O. M. Knyaz'kov, Sov. J. Part. Nucl. **17**, 137 (1986).

[32] D. T. Khoa and G. R. Satchler, Nucl. Phys. A **668**, 3 (2000).

[33] M. Avrigeanu, G. S. Anagnostatos, A. N. Antonov, and J. Giapitzakis, Phys. Rev. C **62**, 017001 (2000); M. Avrigeanu, G. S. Anagnostatos, A. N. Antonov, and V. Avrigeanu, Int. J. Mod. Phys. E **11**, 249 (2002); M. Avrigeanu, A. N. Antonov, H. Lenske, and I. Stetcu, Nucl. Phys. A **693**, 616 (2001).

[34] D. T. Khoa, G. R. Satchler, and W. von Oertzen, Phys. Rev. C **56**, 954 (1997).

[35] M. Y. M. Hassan, M. Y. H. Farag, E. H. Esmael, and H. M. Maridi, Phys. Rev. C **79**, 014612 (2009).

[36] M. Y. H. Farag, E. H. Esmael, and H. M. Maridi, Eur. Phys J. A **48**, 154 (2012).

[37] M. Y. H. Farag, E. H. Esmael, and H. M. Maridi, Phys. Rev. C **90**, 034615 (2014).

[38] K. V. Lukyanov, E. V. Zemlyanaya, and V. K. Lukyanov, Phys. At. Nucl. **69**, 240 (2006); JINR Preprint P4-2004-115, Dubna, 2004.

[39] P. Shukla, Phys. Rev. C **67**, 054607 (2003).

[40] M. Y. H. Farag, E. H. Esmael, and H. M. Maridi, Eur. Phys J. A **50**, 106 (2014).

[41] K. V. Lukyanov, V. K. Lukyanov, E. V. Zemlyanaya, A. N. Antonov, and M. K. Gaidarov, Eur. Phys. J. A **33**, 389 (2007).

[42] V. K. Lukyanov, D. N. Kadrev, E. V. Zemlyanaya, A. N. Antonov, K. V. Lukyanov, and M. K. Gaidarov, Phys. Rev. C **82**, 024604 (2010).

[43] V. K. Lukyanov, E. V. Zemlyanaya, K. V. Lukyanov, D. N. Kadrev, A. N. Antonov, M. K. Gaidarov, and S. E. Massen, Phys. Rev. C **80**, 024609 (2009).

[44] V. K. Lukyanov, D. N. Kadrev, E. V. Zemlyanaya, K. V. Lukyanov, A. N. Antonov, M. K. Gaidarov, and K. Spasova, Phys. Rev. C **88**, 034612 (2013); V. K. Lukyanov, E. V. Zemlyanaya, K. V. Lukyanov, D. N. Kadrev, A. N. Antonov, M. K. Gaidarov, and K. Spasova, Phys. At. Nucl. **75**, 1407 (2012).

[45] K. V. Lukyanov, JINR Comm. R11-2007-38, Dubna, 2007.

[46] R. J. Glauber, in *Lectures in Theoretical Physics* (Interscience, New York, 1959), p. 315.

[47] A. G. Sitenko, Ukr. Fiz. J. **4**, 152 (1959).

[48] S. Karataglidis, P. G. Hansen, B. A. Brown, K. Amos, and P. J. Dortmans, Phys. Rev. Lett. **79**, 1447 (1997).

[49] S. Karataglidis, P. J. Dortmans, K. Amos, and C. Bennhold, Phys. Rev. C **61**, 024319 (2000).

[50] S. C. Pieper, K. Varga, and R. B. Wiringa, Phys. Rev. C **66**, 044310 (2002).

[51] S. C. Pieper (private communication).

[52] P. Descouvemont, Nucl. Phys. A **615**, 261 (1997).

[53] M. Fukuda, T. Ishihara, N. Inabe, T. Kubo, H. Kumagai, T. Nakagawa, Y. Yano, I. Tanihata, M. Adachi, K. Asahi, M. Kouguchi, M. Ishihara, H. Sagawa, and S. Shimoura, Phys. Lett. B **268**, 339 (1991).

[54] N. Fukuda, T. Nakamura, N. Aoi, N. Imai, M. Ishihara, T. Kobayashi, H. Iwasaki, T. Kubo, A. Mengoni, M. Notani, H. Otsu, H. Sakurai, S. Shimoura, T. Teranishi, Y. X. Watanabe, and K. Yoneda, Phys. Rev. C **70**, 054606 (2004).

[55] E. Cravo, R. Crespo, A. M. Moro, and A. Deltuva, Phys. Rev. C **81**, 031601(R) (2010).

[56] H. Sagava, B. A. Brown, and H. Esbensen, Phys. Lett. B **309**, 1 (1993).
[57] T. Nakamura *et al.*, Phys. Lett. B **331**, 296 (1994).
[58] X. Campy and A. Bonyssy, Phys. Lett. B **73**, 263 (1978).
[59] J. W. Negele and D. Vautherin, Phys. Rev. C **5**, 1472 (1972).
[60] S. K. Charagi and S. K. Gupta, Phys. Rev. C **41**, 1610 (1990); **46**, 1982 (1992).
[61] P. D. Kunz and E. Rost, in *Computational Nuclear Physics*, edited by K. Langanke *et al.* (Springer-Verlag, New York, 1993), Vol. 2, p. 88.
[62] V. V. Burov and V. K. Lukyanov, Preprint JINR, R4-11098, 1977, Dubna; V. V. Burov, D. N. Kadrev, V. K. Lukyanov, and Yu. S. Pol', Phys. At. Nucl. **61**, 525 (1998); V. K. Lukyanov *et al.*, *ibid.* **67**, 1282 (2004).
[63] V. Lapoux *et al.*, Phys. Lett. B **658**, 198 (2008).
[64] V. K. Lukyanov, D. N. Kadrev, E. V. Zemlyanaya, A. N. Antonov, K. V. Lukyanov, K. Spasova, and M. K. Gaidarov, Bull. Russ. Acad. Sci.: Phys. **78**, 1363 (2014).
[65] E. A. Romanovsky *et al.*, Bull. Russ. Acad. Sci.: Phys. **62**, 150 (1998).
[66] K. T. Schmitt *et al.*, Phys. Rev. C **88**, 064612 (2013).
[67] H. Esbensen, Phys. Rev. C **53**, 2007 (1996).
[68] D. R. Thompson, M. Le Mere, and Y. C. Tang, Nucl. Phys. A **286**, 53 (1977); Y. C. Tang, M. Le Mere, and D. R. Thompson, Phys. Rep. **47**, 167 (1978).
[69] J. D. Patterson and R. J. Peterson, Nucl. Phys. A **717**, 235 (2003).
[70] R. de Diego, J. M. Arias, J. A. Lay, and A. M. Moro, Phys. Rev. C **89**, 064609 (2014).